


Synthesis, Structure, and Properties of a T-Shaped 14-Electron Stiboranyl-Gold Complex

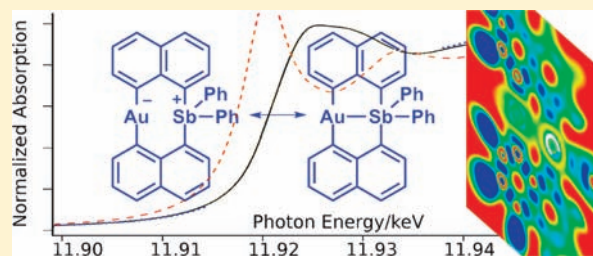
Casey R. Wade,[†] Tzu-Pin Lin,[†] Ryan C. Nelson,[‡] Elizabeth A. Mader,[‡] Jeffrey T. Miller,^{*,‡} and François P. Gabbaï^{*,†}

[†]Department of Chemistry, Texas A&M University, College Station, Texas 77843-3255, United States

[‡]Chemical Sciences and Engineering Division, Argonne National Laboratory, Argonne, Illinois 60439-4837, United States

 Supporting Information

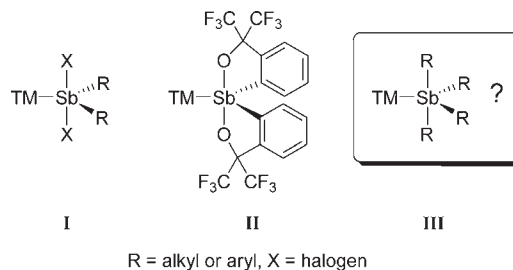
ABSTRACT: A cyclic stiboranyl-gold complex (**1**) supported by two 1,8-naphthalenediyl linkers has been synthesized and structurally characterized. The gold atom of this complex adopts a T-shaped geometry and is separated from the antimony center by only 2.76 Å. Surprisingly, the trivalent gold atom of this complex is involved in an aurophilic interaction, a phenomenon typically only observed for monovalent gold complexes. This phenomenon indicates that the stiboranyl ligand possesses strong σ -donating properties making the trivalent gold atom of **1** electron rich. This view is supported by DFT calculations as well as Au L₃- and Sb K-edge XANES spectra which reveal that **1** may also be described as an aurate-stibonium derivative. In agreement with this view, complex **1** shows no reactivity toward the halides Cl⁻, Br⁻, and I⁻. It does, however, rapidly react with F⁻ to form an unprecedented anionic aurate fluorostiborane complex ([**2**]⁻) which has been isolated as the tetra-*n*-butylammonium salt. The increased coordination number of the antimony center in this anionic complex ([**2**]⁻) does not notably affect the Au–Sb separation (2.77 Å) or the geometry at the gold atom which remains T-shaped.



INTRODUCTION

T-shaped 14-electron transition metal complexes constitute an interesting class of compounds because of their inherent unsaturation.¹ Such complexes can be stabilized through the use of noncoordinating anions and/or bulky ligands, which sterically hinder the coordination of a fourth ligand to the unsaturated transition metal center.² Another useful strategy relies on the use of silyl³ or boryl ligands⁴ whose strong σ -donating properties can be used to increase the lability of the trans-ligand. The properties of these ligands can be illustrated by a series of cationic T-shaped bis(phosphine)platinum boryl derivatives, which can be formed, albeit when a noncoordinating anion is employed.⁵ The preponderance of silyl and boryl ligands for the stabilization of T-shaped 14-electron complexes has led us to question whether other main group ligands could also behave as strong σ -donors. In search of such ligands, we were drawn by the fact that antimony species such as Ph₄SbX (X = halogen) become increasingly ionic as the size of the halogen increases.⁶ This behavior, which is promoted by the electropositive character of antimony, suggested to us that a tetraorganostiboranyl (R₄Sb) ligand⁷ may possess strong σ -donating properties and may be well-adapted for the formation of T-shaped 14-electron transition metal complexes.

In contrast to triaryl and trialkyl stibines which have enjoyed a wide precedent in coordination chemistry,⁸ few transition metal complexes possessing stiboranyl ligands have been isolated. Most examples of such complexes consist of derivatives of type I and II

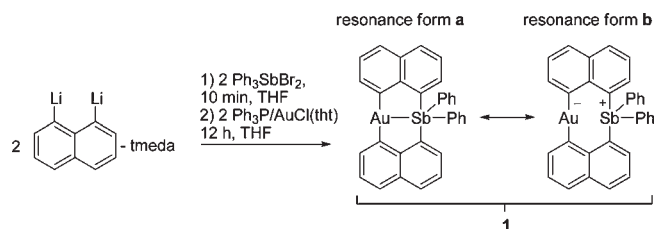


which feature R₂X₂Sb (type I)^{7a,b} or R₂R^fO₂Sb (type II)^{7c-f} stiboranyl ligands (R = alkyl or aryl, X = halogen, R^fO = fluorinated alkoxy group). A noteworthy feature of complexes of type I and II pertains to the presence of electronegative halogen or alkoxy groups whose electron-withdrawing character may limit the σ -donating properties of the stiboranyl group. While several derivatives of type I and II have been previously described,⁷ transition metal complexes featuring the more σ -donating tetraorganostiboranyl (R₄Sb) ligands (type II) have to our knowledge never been reported, possibly because of a lack of adequate synthetic approaches.

Seeking inspiration from a series of reports dealing with the coordination of σ -acceptor ligands to late transition metal complexes,⁹ it occurred to us that a tetraorganostiboranyl

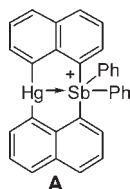
Received: February 3, 2011

Published: May 13, 2011

Scheme 1. Synthesis of the Stiboranyl–Gold Complex **1**^a

^a tmeda = tetramethylethylenediamine, THF = tetrahydrofuran, tht = tetrahydrothiophene.

complex could be approached, at least conceptually, by coordination of a tetraorganostibonium ion to an electron-rich transition metal complex. Inspired by this idea and having recently succeeded in the isolation of **A**, a compound best described as a mercury stibonium derivative,¹⁰ we have now chosen to investigate the synthesis of late transition analogs of this mercury derivative.



In this paper, we report the first successful implementation of this approach with the synthesis and characterization of a T-shaped, 14-electron, trivalent stiboranyl-gold complex.¹¹ Through a combination of experimental, spectroscopic, and computational methods, we show that the stiboranyl ligand present in this complex possesses strong σ -donating properties and renders the gold atom of this complex unusually electron rich.

RESULTS AND DISCUSSION

Synthesis Structure and Bonding. Reaction of Ph_3SbBr_2 with 1,8-dilithionaphthalene and, subsequently, $\text{AuCl}(\text{tht})$ and Ph_3P in THF afforded, after recrystallization from CH_2Cl_2 , the stiboranyl-gold complex **1** in 37% yield (Scheme 1). This compound, which can be represented on the basis of two resonance structures (form a and b), is air stable. It has been characterized by conventional means including ^1H NMR spectroscopy which confirms the unsymmetrical substitution of the naphthalenediyl backbones. Compound **1** crystallizes in the space group $P\bar{1}$ with two independent molecules in the asymmetric unit (Figure 1). The two independent molecules possess almost identical structures and feature a short Au–Sb bond distance of 2.76 Å (av.). This bond distance, which is essentially equal to the sum of the covalent radii of the two elements (2.75 Å),¹² is only marginally longer than the Au–Sb bonds found in stibine–gold complexes such as $[\text{Au}(\text{SbMe}_3)_2][\text{ClO}_4]$ (2.58 Å)¹³ or $[\text{Au}(\text{SbPh}_3)_4][\text{ClO}_4]$ (2.656–2.658 Å).¹⁴ The short Au–Sb bond indicates a strong interaction. This view is reinforced by a comparison of **1** with its isoelectronic mercury analogue **A**.¹⁰ Indeed, despite the similarity of the covalent radii of mercury (1.32 Å) and gold (1.36 Å),¹² the average Au–Sb bond distance in **1** (2.76 Å, respectively) is markedly shorter than the $\text{Hg}\rightarrow\text{Sb}$ bond observed in **A** (3.0601(7) Å). Owing to the presence of this Au–Sb bond, the gold atom adopts a T-shaped

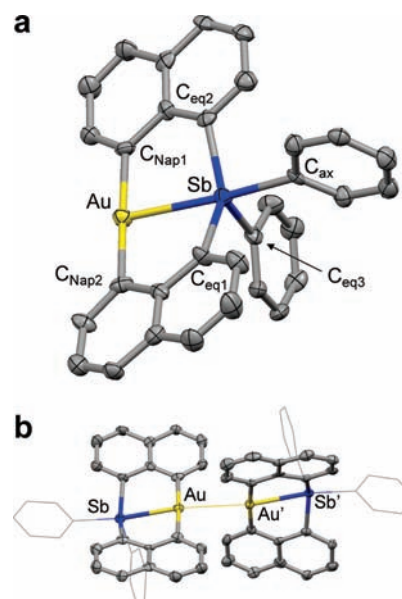


Figure 1. Crystal structure of (a) one of the independent molecules of **1** and (b) both independent molecules showing the presence of the aurophilic contact. Thermal ellipsoids are drawn at the 50% probability level. Hydrogen atoms are omitted for clarity. Selected bond lengths (Å) and angles (deg) (the metrical parameters of the second independent molecule are given in brackets) for **1**: Au–Sb 2.7486(7) [2.7746(8)], Au–Au' 3.2551(7); $\text{C}_{\text{Nap1}}\text{–Au–C}_{\text{Nap2}}$ 177.0(3) [172.4(3)], $\text{C}_{\text{Nap1}}\text{–Au–Sb}$ 88.8(3) [88.6(2)], $\text{C}_{\text{Nap2}}\text{–Au–Sb}$ 89.2(3) [88.5(3)], Au–Sb– C_{ax} 172.0(2) [171.4(3)].

geometry as confirmed by the average $\text{C}_{\text{Nap}}\text{–Au–Sb}$ and $\text{C}_{\text{Nap1}}\text{–Au–C}_{\text{Nap2}}$ angles of 88.8° and 174.7°, respectively. Accordingly, the antimony atom displays a distorted trigonal bipyramidal geometry with the gold atom in an axial position. The Au–Sb– C_{ax} angle of 171.8° (av.) as well as the sum of the $\text{C}_{\text{eq}}\text{–Sb–C}_{\text{eq}}$ angles of 356.3° (av.) supports this view (Figure 1). A last point of interest in this structure relates to the presence of an aurophilic interaction of 3.2551(7) Å which connects the two independent molecules (Figure 1). The formation of such a contact as well as the perpendicular orientation of the two monomers is reminiscent of monovalent gold compounds such as $\text{Me}_3\text{PAu}^{15}$ or $(2,6\text{-Me}_2\text{C}_6\text{H}_3\text{NC})\text{AuCl}^{16}$ which also form perpendicular aurophilic dimers with Au–Au distances of 3.168(1) and 3.3555(5) Å, respectively.¹⁷ Aurophilic contacts involving trivalent species are limited to two examples which each display stacked square planar units and Au–Au distances longer than 3.5 Å.¹⁸ This structural analysis indicates that the gold atom of **1** may be as electron rich as that in gold monohalide complexes. Thus, despite the short Au–Sb bond which supports the presence of a covalent linkage between the two atoms as represented in resonance form a, the gold atom behaves as that of simple monovalent complexes, pointing to the relevance of resonance form b.

X-ray Absorption Spectroscopy. To gather additional information about the electronic structure of **1**, we decided to study the atomic properties of the gold nucleus in **1** by measuring its room temperature, solid state Au L_3 -X-ray Absorption Near Edge Structure (XANES) spectrum along with that of two reference compounds, namely $\text{AuCl}(\text{PPh}_3)$ and CsAuCl_4 (Figure 2). In agreement with the trend established for gold compounds at the L_3 -edge,¹⁹ we observed that the edge position of the trivalent

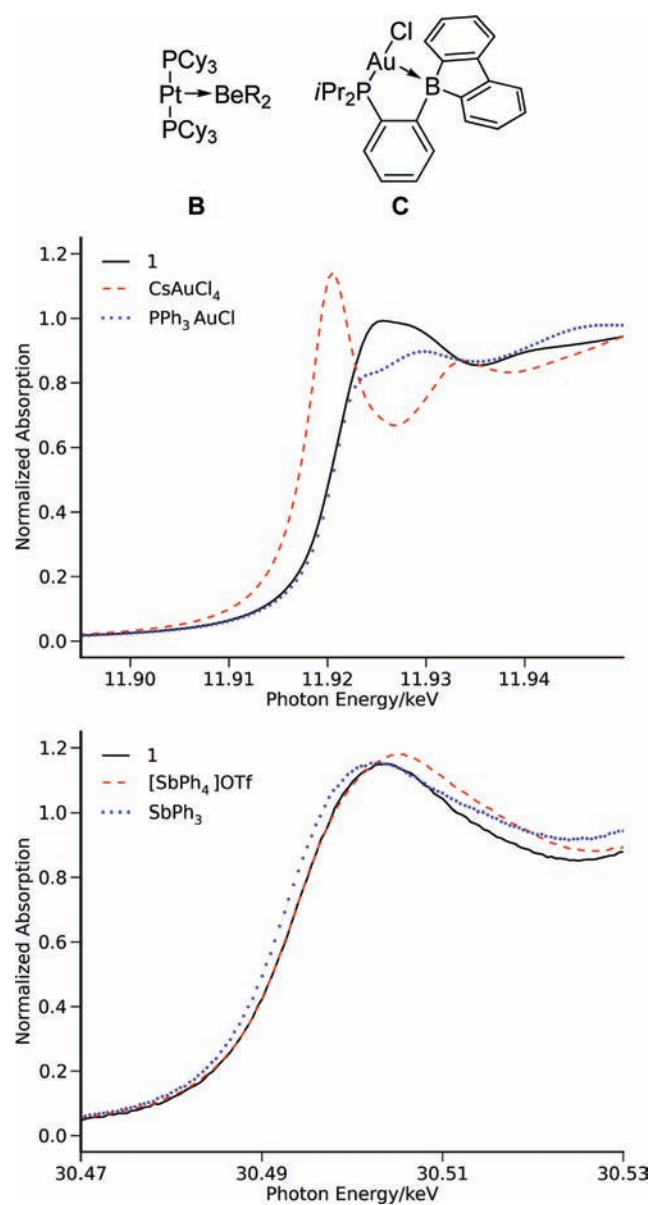


Figure 2. Solid-State XANES spectrum: (Top) Au L₃-edge of **1** (—) compared to reference complexes of Au³⁺ (CsAuCl₄, ---) and Au¹⁺ (AuCl(PPh₃), ···). (Bottom) Sb K-edge of **1** (—) compared to reference complexes of Sb⁵⁺ ([SbPh₄][OTf], ---) and Sb³⁺ (SbPh₃, ···).

gold reference CsAuCl₄ (11918.9 eV) is at lower energy than that measured for the monovalent gold reference compounds AuCl(PPh₃) (11921.2 eV). Notably, the Au L₃ XANES spectrum of **1** shows an edge position of 11921.4 eV, a value very close to that measured for the monovalent gold reference AuCl(PPh₃). Next, we decided to study compound **1** by Sb K-edge-XANES spectroscopy. The Sb K-edge of XANES spectra is typically dominated by 1s→p transitions whose energy increases with the valence of the antimony atom.²⁰ Our measurements shown in Figure 2 indicate that the Sb K-edge of **1** (30493.3 eV) is essentially identical to that measured for the stibonium salt [SbPh₄][OTf] (30493.3 eV) and at higher energy than that of the trivalent reference compound SbPh₃ (30492.0 eV). Although only a small energy difference (1.3 eV) was observed between the Sb K-edge of SbPh₃ and those of **1** and [SbPh₄][OTf], multiple

recordings of each spectra showed very little variance (less than 0.1 eV) confirming that the difference is not the result of random measurement error. Collectively, these results indicate that an aurate-stibonium resonance structure (form **b**, Scheme 1) for **1** must be considered, possibly as the most important contributor. It follows that **1** is closely related to a series of complexes such as **B**²¹ and **C**,²² which have been described according to a donor–acceptor formalism with the late transition metal center acting as a σ -donor and the main group element as a σ -acceptor ligand.^{9,23}

Computational Studies. To better understand the electronic structure of **1**, we carried out DFT calculations using the ADF program. All calculations were carried out at the BP86/TZP level of theory using the zero-order regular approximation (ZORA). Geometry optimization starting from the solid state structure of one of the independent molecules of **1** afforded a structure that is in excellent agreement with that observed experimentally (see Supporting Information). A first assessment of the nature of the Au–Sb bond was derived from the Electron Localization Function (ELF), a function which can be used to map the electron pair localization in a molecule.²⁴ The ELF map of **1** is characterized by a continuum of relatively elevated ELF values along the Au–Sb vector, indicating some degree of electron sharing between the two heavy atoms (Figure 3). Additional insight into the nature of the Au–Sb bond was provided by a molecular orbital analysis. Compound **1** was subjected to a Boys localization analysis because of extensive delocalization of the occupied Kohn–Sham orbitals. This analysis identifies two C–Au σ -bonding orbitals connecting the Au atom to the two naphthalene ligands. These σ -orbitals show little polarization, in agreement with the low electronegativity difference between carbon ($\chi = 2.54$) and gold ($\chi = 2.55$). By contrast, the only orbital of σ -symmetry oriented along the Au–Sb axis is very strongly polarized toward the gold atom with very little contribution from the antimony atom. This observation supports the notion that the stiboranyl ligand acts as a strong σ -donor. It also lends further support to the relevance of the aurate–stibonium contribution (resonance form **b** in Scheme 1) in the description of **1**. This view is further supported by the electrostatic potential map of **1** which shows a clear accumulation of negative charge on the gold atom (see Supporting Information). Collectively these computational results show that the Au–Sb bond is highly polarized, making the trivalent gold center electron rich.

Photophysical Properties. The electronic absorption spectrum of **1** in CH₂Cl₂ displays a broad band spanning the 350–440 nm range (Figure 4). This low energy feature is attributed to a transition from the naphthalene-based HOMO to the LUMO which bears a significant contribution from a gold 6p and Sb–C_{Ph} σ^* orbitals (Figure 4). The solid state emission spectrum of **1** measured at 77 K shows a broad emission centered at around 660 nm (figure 4). This band is not observed at room temperature suggesting that it corresponds to a triplet excited state arising from a gold heavy atom effect. This view is confirmed by the excited state lifetime of 6.8 μ s which is comparable to that observed for other aurated aromatic derivatives.²⁵ Oxygen-free solutions of **1** in CH₂Cl₂ are not visibly luminescent at room temperature. Upon freezing, however, these solutions give rise to a bright orange emission centered at 560 nm. In turn, the emission of **1** in frozen solution is distinctly blue-shifted when compared to that of the solid state, a phenomenon that we assign to the absence of aurophilic interactions under these conditions.

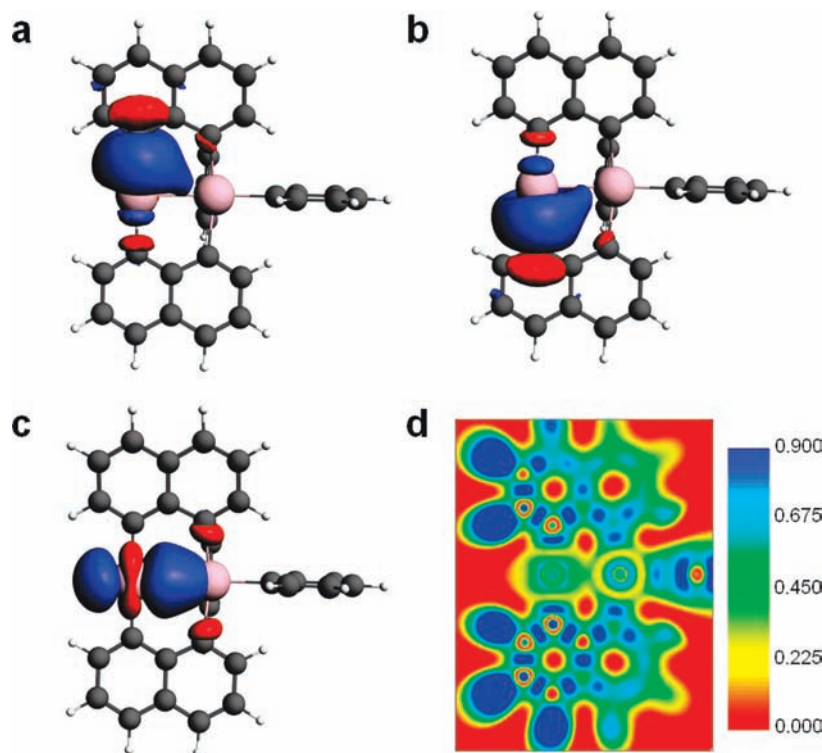


Figure 3. (a–c) Gold-centered Boys orbitals for **1** (drawn with a 0.02 isodensity value). (d) Plot of the electron localization function for **1**.

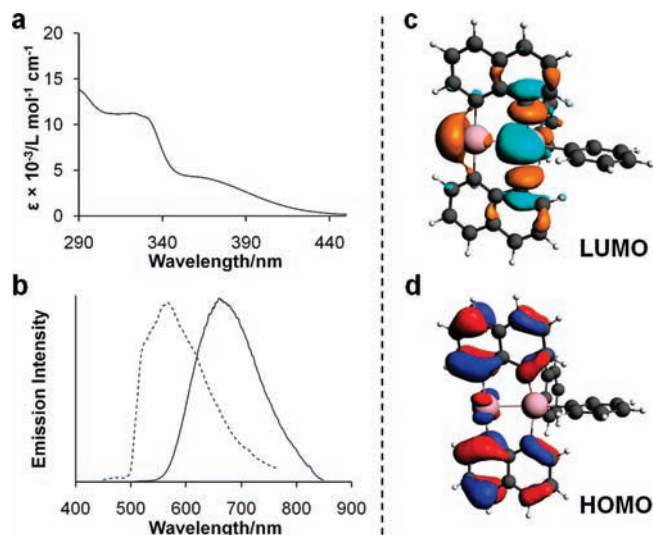
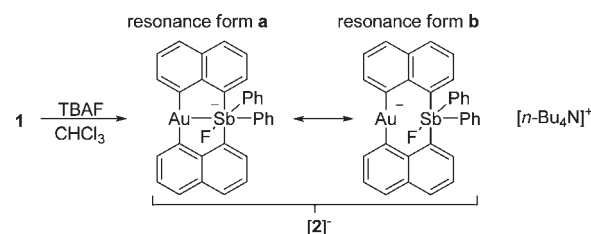


Figure 4. (a) UV–vis absorption spectra of **1** (—) in CH_2Cl_2 , (b) Low temperature (77 K) emission spectra of **1** in the solid state (—) and frozen CH_2Cl_2 solution (·····). (c,d) Frontier orbitals of **1** (drawn with a 0.02 isodensity value).

Reactions with Halide Ions. In line with an accumulation of electron density on the gold atom, and hence the strong σ -donating properties of the stiboranyl ligand, the gold atom of **1** shows no affinity for chloride, bromide, or iodide anions in CDCl_3 . These NMR experiments also showed no measurable interaction between the halide anions and the antimony center of **1**. Interestingly, however, **1** quickly reacts with tetra-*n*-butylammonium fluoride (TBAF) to form an auroated fluoroantimonate anion ($[\mathbf{2}]^-$) which has been isolated as the tetra-*n*-butylammonium

Scheme 2. Synthesis of $[\mathbf{2}]^-$



^a TBAF = tetra-*n*-butylammonium fluoride.

salt (Scheme 2). Evidence for the formation of an Sb–F bond rather than a Au–F bond was provided by the detection of a ^{19}F NMR signal (in acetone- d_6) at -41 ppm, a chemical shift close to that observed for Me_4SbF .²⁶ The selectivity of the antimony center for fluoride over the larger halides is a well documented phenomenon which can be assigned to the increased contribution of the stibonium halide form as the size of the halogen increases.²⁷ Formation of $[\mathbf{2}]^-$ can also be monitored by UV–vis spectroscopy which indicates that the fluoride binding to the antimony quenches the low energy band present in the spectrum of **1** (Figure 5). This observation can be rationalized by an increase in the energy of the LUMO of $[\mathbf{2}]^-$ caused by anion coordination. While DFT calculations (BP86/TZP level of theory with ZORA) indicate that the makeup of this orbital remains similar to that of **1** (Figure 5), this perturbation causes the HOMO–LUMO transition to shift to higher energies. In line with this argument, the UV–vis spectrum of $[\mathbf{2}]^-$ shows the emergence of a new absorption band centered at around 310 nm.

Recrystallization of $[\mathbf{2}]^-$ from THF/toluene (1:1) afforded colorless, plate-like crystals that are not luminescent.

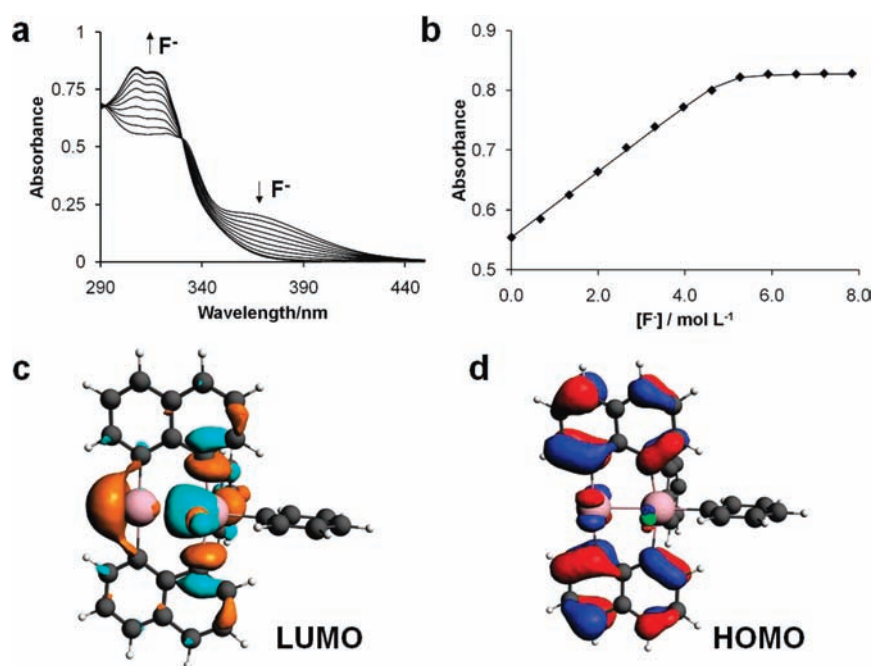


Figure 5. (a) Spectral changes in the UV–vis absorption spectra of **1** (5.0×10^{-5} M in CH_2Cl_2) upon incremental addition of a TBAF solution (4.0×10^{-3} M in CH_2Cl_2). (b) Plot of the absorbance monitored at 314 nm versus $[\text{F}^-]$. The curve was fit to a 1:1 binding model to yield a calculated fluoride binding constant $K = 1.0 \times 10^7 \text{ M}^{-1}$. (c,d) Frontier orbitals of $[\mathbf{2}]^-$ (drawn with a 0.02 isodensity value).

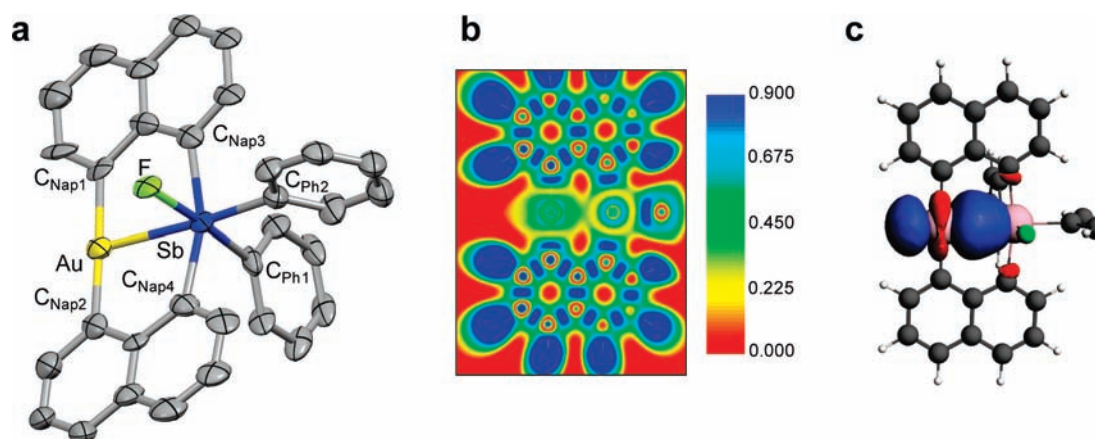


Figure 6. (a) Crystal structure of $[\mathbf{2}]^-$ in the $[\textit{n}\text{-Bu}_4\text{N}][\mathbf{2}]$ salt. Only one of the independent molecules is shown. Thermal ellipsoids are drawn at the 50% probability. Hydrogen atoms are omitted for clarity. Selected bond lengths (\AA) and angles (deg) (the metrical parameters of the second independent molecule are given in brackets). $[\mathbf{2}]^-$: Au–Sb 2.7694(8) [2.7728(9)], Sb–F 2.091(5) [2.060(5)]; $\text{C}_{\text{Nap1}}\text{–Au–C}_{\text{Nap2}}$ 179.2(4) [177.3(3)], $\text{C}_{\text{Nap1}}\text{–Au–Sb}$ 89.9(3) [91.4(3)], $\text{C}_{\text{Nap2}}\text{–Au–Sb}$ 90.4(2) [89.4(3)], Au–Sb– C_{Ph2} 170.4(3) [174.9(3)], F–Sb– C_{Ph1} 174.5(3) [174.9(3)], $\text{C}_{\text{Nap3}}\text{–Sb–C}_{\text{Nap4}}$ 164.0(4) [162.9(4)]. (b) Plot of the Electron Localization Function for $[\mathbf{2}]^-$. (c) Gold-centered Boys orbitals for $[\mathbf{2}]^-$ (drawn with a 0.02 isodensity value).

The salt crystallizes in the space group $P\bar{1}$ with two independent molecules in the asymmetric unit. The structure of $[\mathbf{2}]^-$ shows fluoride coordination to the antimony center with an average Sb–F bond distance of 2.08(2) \AA (Figure 6). This Sb–F distance is similar to that observed in Ph_4SbF (2.0530(8) \AA)²⁷ or Ph_3MeSbF (2.069(3) \AA).²⁸ Fluoride coordination results in a nearly octahedral geometry around antimony with average angles of 174.7° for $\text{C}_{\text{Ph1}}\text{–Sb–F}$, 172.6° for $\text{C}_{\text{Ph2}}\text{–Sb–Au}$, and 163.4° for $\text{C}_{\text{Nap1}}\text{–Sb–C}_{\text{Nap2}}$. The coordination environment of the Au atom remains T-shaped with average $\text{C}_{\text{Naph}}\text{–Au–Sb}$ and $\text{C}_{\text{Nap1}}\text{–Au–C}_{\text{Nap2}}$ angles of 90.3°

and 178.2°, respectively. The Au–Sb distance of 2.771(2) \AA (av.) is virtually unchanged when compared to that in **1**. Inspection of the ELF map and Boys orbitals calculated for $[\mathbf{2}]^-$ shows that they are strikingly similar to those of **1** thus indicating that the nature of the Au–Sb bond is not significantly altered by coordination of a fluoride anion to the antimony center (Figure 6). In turn, compound $[\mathbf{2}]^-$ can also be described according to two resonance structures, the first one corresponding to an aurated antimonate anion (resonance form a), the second one to an aurate fluorostiborane derivative (resonance form b).

CONCLUSIONS

We have prepared and structurally characterized the first example of a stiboranyl-gold complex (**1**). The structural and computational results that we have obtained for this compound indicate that tetraorganostiboranyl ligands have strong σ -donating properties. These strong σ -donating properties lead to an accumulation of electron density on the gold center, giving rise in the case of **1** to the emergence of aurophilicity, a phenomenon typically preponderant in monovalent gold species.¹⁷ Another manifestation of these strong σ -donating properties is the lack of reactivity of the gold center toward halide anions and its stabilization in a T-shaped geometry. These observations, complemented by the results of the XANES measurements and DFT calculations, underscore the importance of a diarylaurate-stibonium resonance structure in the description of complex **1**. Adopting the donor–acceptor formalism that has been recently popularized for late transition metals coordinated to Lewis acidic ligands, we can describe complex **1** as a diarylaurate anion stabilized by partial donation to a Lewis acidic stibonium ligand. The same reasoning can be applied to $[2]^-$, which can be described as a diarylaurate anion intramolecularly stabilized by a Lewis acidic fluorostiborane.^{9,21–23}

EXPERIMENTAL SECTION

General Considerations. Antimony compounds are highly toxic and should be handled cautiously. Triphenylphosphine was purchased from Aldrich. Tetra-*n*-butylammonium fluoride was purchased from Alfa Aesar. 1,8-Dilithionaphthalene·TMEDA,²⁹ triphenyl-dibromoantimony,³⁰ and AuCl(tht)³¹ (tht = tetrahydrothiophene) were prepared according to the reported procedures. All preparations were carried out under an atmosphere of dry N₂ employing either a glovebox or standard Schlenk techniques. Solvents were dried by passing through an alumina column (CH₂Cl₂) or refluxing under N₂ over Na/K (Et₂O, *n*-hexane, and THF). NMR spectra were recorded on a Varian Unity Inova 400 FT NMR (399.59 MHz for ¹H, 375.99 MHz for ¹⁹F, 100.45 MHz for ¹³C) spectrometer at ambient temperature. Chemical shifts are given in ppm and are referenced to residual ¹H and ¹³C solvent signals and external BF₃·Et₂O for ¹⁹F. Elemental analyses were performed by Atlantic Microlab (Norcross, GA).

Synthesis of **1.** A solution of Ph₃SbBr₂ (500 mg, 0.976 mmol) in THF (3 mL) was added dropwise to a solution of 1,8-dilithionaphthalene (250 mg, 0.976 mmol) in THF (2 mL) at ambient temperature. The mixture was allowed to stir for 10 min before adding a solution of AuCl(tht) (313 mg, 0.976 mmol) and Ph₃P (256 mg, 0.976 mmol) in THF (5 mL). The resulting clear yellow solution was layered with Et₂O (5 mL) and hexane (5 mL) and allowed to stand at room temperature. After 2 days, a mixture of yellow and colorless crystals was obtained. Both types of crystals were suitable for X-ray diffraction, which identified the colorless crystals as AuBr(Ph₃P)₂ and the yellow crystals as complex **1**. Multiple recrystallizations of the crude mixture from hot CH₂Cl₂ (10 mL) provided a pure sample of **1** (130 mg, 37% yield). ¹H NMR (399.59 MHz; CDCl₃): δ 8.02 (d, 2H, Naph-CH, ³J_{H-H} = 7.81 Hz), 7.89 (dd, 2H, Naph-CH, ³J_{H-H} = 6.6 Hz, ⁴J_{H-H} = 1.2 Hz), 7.77 (dd, 2H, Naph-CH, ³J_{H-H} = 8.1 Hz, ⁴J_{H-H} = 1.2 Hz), 7.64–7.58 (m, 4H, Naph-CH), 7.44 (t, 2H, *p*-Ph-CH, ³J_{H-H} = 7.3 Hz), 7.34 (t, 4H, *m*-Ph-CH, ³J_{H-H} = 7.3 Hz), 7.27–7.20 (m, 6H, *o*-Ph-CH and Naph-CH); ¹³C{¹H} NMR (100.45 MHz; CDCl₃): δ 183.71, 145.82, 139.66, 136.68, 135.69, 134.80, 134.62, 134.20, 133.13, 130.49, 129.66, 126.78, 124.33, 124.18. Elemental analysis calculated (%) for C₃₂H₂₂AuSb: C, 52.99; H, 3.06. Found: C, 52.38; H, 3.12.

Synthesis of $[n\text{-Bu}_4\text{N}][2]$. Solid TBAF·3H₂O (4.4 mg, 0.013 mmol) was added to a solution of **1** (10 mg, 0.013 mmol) in CHCl₃ (1 mL).

Upon standing, $[n\text{-Bu}_4\text{N}][2]$ precipitated as a colorless microcrystalline solid which was washed with Et₂O (2 mL) and dried in vacuum to yield 9.1 mg (70%). Crystals of $[n\text{-Bu}_4\text{N}][2]$ suitable for X-ray diffraction were obtained by slow evaporation of a solution of the compound in THF/toluene (1/1 vol). ¹H NMR (399.59 MHz; acetone-*d*₆): δ 7.95 (br, 2H, Ph-CH), 7.75 (d, 2H, Naph-CH, ³J_{H-H} = 7.88 Hz), 7.63 (d, 2H, Naph-CH, ³J_{H-H} = 6.59 Hz), 7.58 (d, 2H, Naph-CH, ³J_{H-H} = 8.06 Hz), 7.42–7.52 (m, 3H, Ph-CH), 7.37 (dd, 2H, Naph-CH, ³J_{H-H} = 8.06, 6.59 Hz), 7.33 (d, 2H, Ph-CH, ³J_{H-H} = 6.96 Hz), 7.07 (t, 2H, Naph-CH, ³J_{H-H} = 6.96 Hz), 6.97 (t, 1H, Ph-CH, ³J_{H-H} = 6.96 Hz), 6.78–6.88 (m, 4H, Naph-CH, Ph-CH), 3.24 (m, 8H, *n*-Bu₄N⁺), 1.63 (m, 8H, *n*-Bu₄N⁺), 1.26 (tq, 8H, *n*-Bu₄N⁺, ³J_{H-H} = 7.51 Hz), 0.88 (t, 8H, *n*-Bu₄N⁺, ³J_{H-H} = 7.33 Hz). ¹³C{¹H} NMR (100.45 MHz; acetone-*d*₆): δ 187.97, 145.86, 137.87, 136.86, 136.37, 135.74, 135.64, 135.08, 134.70, 131.45, 131.32, 130.06, 129.47, 129.03, 127.96, 125.71, 124.07, 123.95, 59.10, 24.33, 20.25, 13.86. ¹⁹F NMR (375.99 MHz; acetone-*d*₆): δ –43.26. HRMS: *m/z* calculated for C₃₂H₂₂FAuSb[–], 743.0409; found, 743.0425.

Computational Details. DFT structural optimizations for **1** and $[2]^-$ were carried out using the ADF program (2008.01).³² All calculations were carried out using the BP86 functional³³ with the all electron TZP basis sets for all atoms.³⁴ These calculations were performed using ZORA.³⁵ Electron localization function (ELF)²⁴ and Boys³⁶ localization were carried out in the ADF program. ELF plots as well as Boys localized orbitals were visualized in the ADFview program. The structure of **C** has been previously optimized at the same level of theory.¹⁰

Crystallographic Measurements. All crystallographic measurements were performed at 110(2) K using a Bruker SMART APEX II diffractometer with a CCD area detector (graphite monochromated Mo K α radiation, λ = 0.71073 Å, ω -scans with a 0.5° step in ω) at 110 K. In each case, a specimen of suitable size and quality was selected and mounted onto a nylon loop. The semiempirical method SADABS was applied for absorption correction. The structures were solved by direct methods and refined by the full-matrix least-squares technique against F^2 with the anisotropic temperature parameters for all non-hydrogen atoms. All H-atoms were geometrically placed and refined in riding model approximation. Data reduction and further calculations were performed using the Bruker SAINT+³⁷ and SHELXTL NT program packages.³⁸

After numerous modeling attempts, heavily disordered solvent molecules in the structure of $[n\text{-Bu}_4\text{N}][2]$ were handled using the Squeeze program implemented in PLATON.³⁹ The program calculated a solvent-accessible volume of 726.9 Å³ (15.68% of the total unit cell volume), which was then removed from subsequent structure factor calculations.

X-ray Absorption Spectroscopy. X-ray absorption measurements were acquired on Materials Research Collaborative Access Team (MR-CAT) beamlines at the Advanced Photon Source, Argonne National Laboratory. The Au L₃-edge (11,919 eV) spectra were acquired on an insertion-device beamline, and measurements of the Sb K-edge (30,491 eV) were made on a bending magnet beamline. In both cases, spectra of elemental foils (Au and Sb, respectively) were collected simultaneously with the sample measurements for energy calibration and multiple scans were taken to ensure spectrum reproducibility.

Insertion-device experiments utilized a cryogenically cooled double-crystal Si (111) monochromator in conjunction with an uncoated glass mirror to minimize the presence of harmonics. The monochromator was scanned continuously during the measurements with data points integrated over 0.6 eV for 0.07 s per data point. Measurements were made in transmission mode with the ionization chambers optimized for the maximum current with linear response (~1010 photons detected/s) using a mixture of nitrogen and helium in the incident X-ray detector and a mixture of ca. 20% argon in nitrogen in the transmission X-ray detector.

Photon energies at the bending magnet were selected using a water-cooled, double-crystal Si(111) monochromator, which was detuned by approximately 50% to reduce harmonic reflections. Measurements were made in transmission mode with argon filled ionization chambers. Data points were acquired in four separate regions (energies relative to the elemental Sb K-edge): a pre-edge region -250 to -30 eV (step size = 10 eV, dwell time = 0.3 s), the XANES region from -30 to $+40$ eV (step size = 0.5 eV, dwell time = 0.2 s), an initial EXAFS region from $+40$ eV to 6 k (step size = 0.07 k, dwell time = 0.5 s), and a final EXAFS region from 6 to 14 k (step size = 0.07 k, dwell time = 0.5 s).

Samples were prepared by pressing ~ 20 mg of finely ground powders of the compounds mixed with silica gel into a 4 mm diameter cylindrical sample holder. Mixtures were made to be approximately 7.5 wt % Au for Au L_{3-} edge and 10 wt % Sb for Sb K-edge, and enough sample was used to obtain a step height of about 1.5. Grinding and sample preparation were done in air, and the sample spectra were acquired in air at room temperature.

In order to determine accurate and reproducible edge energies, the slightly asymmetric, initial positive feature in the first derivative XANES spectrum was fit using a linear combination of two independent Gaussian functions (generally over an energy range of ± 10 eV around the peak). The fitted position of the Gaussian peak that best overlaps with the initial first derivative maximum was then chosen to represent the edge energy.

UV-vis Absorption and Luminescence Measurements.

Electronic absorption spectra were recorded using an Ocean Optics USB4000 spectrometer with an Ocean Optics ISS light source. Steady state emission spectra were collected at room temperature using a PTI QuantaMaster 4 fluorescence spectrophotometer equipped with a Model 810 PMT detector. Solution based samples were prepared at ca. 1 mM concentrations under an atmosphere of N_2 using dry, degassed CH_2Cl_2 . Solid samples were loaded as powders in standard quartz NMR tubes and suspended in the sample cavity to sit at the intersection of the excitation and emission optical paths. Time-resolved phosphorescence lifetime data were collected using a PTI QuantaMaster spectrophotometer equipped with a pulsed Xenon light source and gated PMT detector.

ASSOCIATED CONTENT

S Supporting Information. Crystallographic data (CIF format), computational details, supplementary tables, and figures. This material is available free of charge via the Internet at <http://pubs.acs.org>.

AUTHOR INFORMATION

Corresponding Author

francois@tamu.edu

ACKNOWLEDGMENT

Support by the National Science Foundation (CHE-0646916 and CHE-0952912), the Welch Foundation (A-1423), and Texas A&M University (Davidson Professorship) is gratefully acknowledged. The use of the Advanced Photon Source was supported by the U.S. Department of Energy, Office of Science, Office of Basic Energy Sciences, under Contract DE-AC02-06CH11357. MRCAT operations are supported by the Department of Energy and the MRCAT member institutions. We thank the referees for their help in improving this manuscript.

REFERENCES

- (1) (a) Ingleson, M. J.; Mahon, M. F.; Weller, A. S. *Chem. Commun.* **2004**, 2398–2399. (b) Moncho, S.; Ujaque, G.; Lledos, A.; Espinet, P. *Chem.—Eur. J.* **2008**, *14*, 8986–8994. (c) Chaplin, A. B.; Poblador-Bahamonde, A. I.; Sparkes, H. A.; Howard, J. A. K.; Macgregor, S. A.; Weller, A. S. *Chem. Commun.* **2009**, 244–246.
- (2) (a) Baratta, W.; Stoccoro, S.; Doppiu, A.; Herdtweck, E.; Zucca, A.; Rigo, P. *Angew. Chem., Int. Ed.* **2003**, *42*, 105–109. (b) Lavallo, V.; Canac, Y.; DeHope, A.; Donnadieu, B.; Bertrand, G. *Angew. Chem., Int. Ed.* **2005**, *44*, 7236–7239. (c) Stambuli, J. P.; Incarvito, C. D.; Buehl, M.; Hartwig, J. F. *J. Am. Chem. Soc.* **2004**, *126*, 1184–1194. (d) Yamashita, M.; Hartwig, J. F. *J. Am. Chem. Soc.* **2004**, *126*, 5344–5345.
- (3) (a) Korshin, E. E.; Leitus, G.; Shimon, L. J. W.; Konstantinovskii, L.; Milstein, D. *Inorg. Chem.* **2008**, *47*, 7177–7189. (b) Sangtrirutnugul, P.; Stradiotto, M.; Tilley, T. D. *Organometallics* **2006**, *25*, 1607–1617. (c) Whited, M. T.; Mankad, N. P.; Lee, Y.; Oblad, P. F.; Peters, J. C. *Inorg. Chem.* **2009**, *48*, 2507–2517. (d) Tsay, C.; Mankad, N. P.; Peters, J. C. *J. Am. Chem. Soc.* **2010**, *132*, 13975–13977.
- (4) (a) Spokoyny, A. M.; Reuter, M. G.; Stern, C. L.; Ratner, M. A.; Seideman, T.; Mirkin, C. A. *J. Am. Chem. Soc.* **2009**, *131*, 9482–9483. (b) Segawa, Y.; Yamashita, M.; Nozaki, K. *J. Am. Chem. Soc.* **2009**, *131*, 9201–9203.
- (5) (a) Braunschweig, H.; Green, H.; Radacki, K.; Uttinger, K. *Dalton Trans.* **2008**, 3531–3534. (b) Braunschweig, H.; Radacki, K.; Uttinger, K. *Chem.—Eur. J.* **2008**, *14*, 7858–7866.
- (6) Baker, L.-J.; Rickard, C. E. F.; Taylor, M. J. *Dalton Trans.* **1995**, 2895–2899.
- (7) (a) Malisch, W.; Panster, P. *Angew. Chem., Int. Ed.* **1974**, *13*, 670–672. (b) Malisch, W.; Kaul, H. A.; Gross, E.; Thewalt, U. *Angew. Chem., Int. Ed.* **1982**, *21*, 549–550. (c) Yamamoto, Y.; Okazaki, M.; Wakisaka, Y.; Akiba, K.-y. *Organometallics* **1995**, *14*, 3364–3369. (d) Toyota, K.; Yamamoto, Y.; Akiba, K.-Y. *Chem. Lett.* **1999**, 783–784. (e) Toyota, K.; Yamamoto, Y.; Akiba, K.-y. *Organometallics* **2000**, *19*, 5134–5142. (f) Toyota, K.; Wakisaka, Y.; Yamamoto, Y.; Akiba, K.-y. *Organometallics* **2000**, *19*, 5122–5133.
- (8) (a) Levason, W.; Reid, G. *Coord. Chem. Rev.* **2006**, *250*, 2565–2594. (b) Levason, W.; McAuliffe, C. A. *Acc. Chem. Res.* **1978**, *11*, 363–368.
- (9) (a) Parkin, G. *Organometallics* **2006**, *25*, 4744–4747. (b) Hill, A. F. *Organometallics* **2006**, *25*, 4741–4743. (c) Braunschweig, H.; Dewhurst, R. D.; Schneider, A. *Chem. Rev.* **2010**, *110*, 3924–3957. (d) Amgoune, A.; Bourissou, D. *Chem. Commun.* **2011**, 47, 859–871. (e) Bouhadir, G.; Amgoune, A.; Bourissou, D. *Adv. Organomet. Chem.* **2010**, *58*, 1–107.
- (10) Lin, T.-P.; Wade, C. R.; Pérez, L. M.; Gabbai, F. P. *Angew. Chem., Int. Ed.* **2010**, *49*, 6357–6360.
- (11) The term “trivalent” reflects the fact the gold atom uses three of its electrons in bonding. The use of this term does not necessarily imply that the gold atom is in the +III oxidation state. For an exhaustive discussion of the valence concepts, please consult the following reference: Parkin, G. *J. Chem. Educ.* **2006**, *83*, 791–799.
- (12) Cordero, B.; Gomez, V.; Platero-Prats, A. E.; Reyes, M.; Echeverria, J.; Cremades, E.; Barragan, F.; Alvarez, S. *Dalton Trans.* **2008**, 2832–2838.
- (13) Bojan, V. R.; Fernández, E. J.; Laguna, A.; López-de-Luzuriaga, J. M.; Monge, M.; Olmos, M. E.; Puelles, R. C.; Silvestru, C. *Inorg. Chem.* **2010**, *49*, 5530–5541.
- (14) Jones, P. G. *Acta Crystallogr., Sect. C: Cryst. Struct. Commun.* **1992**, *48*, 1487–1488.
- (15) Ahrlund, S.; Dreisch, K.; Noren, B.; Oskarsson, A. *Acta Chem. Scand., Ser. A* **1987**, *41*, 173–177.
- (16) Mathieson, T. J.; Langdon, A. G.; Milestone, N. B.; Nicholson, B. K. *J. Chem. Soc., Dalton Trans.* **1999**, 201–207.
- (17) Schmidbaur, H.; Schier, A. *Chem. Soc. Rev.* **2008**, *37*, 1931–1951.
- (18) (a) Doerr, L. H. *Dalton Trans.* **2010**, 39, 3543–3553. (b) Hayoun, R.; Zhong, D. K.; Rheingold, A. L.; Doerr, L. H. *Inorg. Chem.* **2006**, *45*, 6120–6122. (c) Klapoetke, T. M.; Krumm, B.; Galvez-Ruiz, J.-C.; Noeth, H. *Inorg. Chem.* **2005**, *44*, 9625–9627.

- (19) (a) Elder, R. C.; Eidsness, M. K.; Heeg, M. J.; Tepperman, K. G.; Shaw, C. F. In *ACS Symposium Series 209*; Lippard, S. J., Ed.; American Chemical Society: Washington, DC, 1984; pp 385–400. (b) Elder, R. C.; Eidsness, M. K. *Chem. Rev.* **1987**, *87*, 1027–1046. (c) Watkins, J. W.; Elder, R. C.; Greene, B.; Darnall, D. W. *Inorg. Chem.* **1987**, *26*, 1147–1151. (d) Gardea-Torresdey, J. L.; Tiemann, K. J.; Gamez, G.; Dokken, K.; Cano-Aguilera, I.; Furenlid, L. R.; Renner, M. W. *Environ. Sci. Technol.* **2000**, *34*, 4392–4396. (e) Messori, L.; Balerna, A.; Ascone, I.; Castellano, C.; Gabbiani, C.; Casini, A.; Marchioni, C.; Jaouen, G.; Congiu Castellano, A. *J. Biol. Inorg. Chem.* **2011**, *16*, 491–499.
- (20) (a) Fawcett, S. E.; Gordon, R. A.; Jamieson, H. E. *Am. Mineral.* **2009**, *94*, 1377–1387. (b) Scheinost, A. C.; Rossberg, A.; Vantelon, D.; Xifra, I.; Kretzschmar, R.; Leuz, A.-K.; Funke, H.; Johnson, C. A. *Geochim. Cosmochim. Acta* **2006**, *70*, 3299–3312.
- (21) Braunschweig, H.; Gruss, K.; Radacki, K. *Angew. Chem., Int. Ed.* **2009**, *48*, 4239–4241.
- (22) Bontemps, S.; Bouhadir, G.; Miqueu, K.; Bourissou, D. *J. Am. Chem. Soc.* **2006**, *128*, 12056–12057.
- (23) (a) Hill, A. F.; Owen, G. R.; White, A. J. P.; Williams, D. J. *Angew. Chem., Int. Ed.* **1999**, *38*, 2759–2761. (b) Figueroa, J. S.; Melnick, J. G.; Parkin, G. *Inorg. Chem.* **2006**, *45*, 7056–7058. (c) Pang, K.; Quan, S. M.; Parkin, G. *Chem. Commun.* **2006**, 5015–5017. (d) Landry, V. K.; Melnick, J. G.; Buccella, D.; Pang, K.; Ulichny, J. C.; Parkin, G. *Inorg. Chem.* **2006**, *45*, 2588–2597. (e) Braunschweig, H.; Gruss, K.; Radacki, K. *Angew. Chem., Int. Ed.* **2007**, *46*, 7782–7784. (f) Sircoglou, M.; Bontemps, S.; Mercy, M.; Saffon, N.; Takahashi, M.; Bouhadir, G.; Maron, L.; Bourissou, D. *Angew. Chem., Int. Ed.* **2007**, *46*, 8583–8586. (g) Fox, B. J.; Millard, M. D.; DiPasquale, A. G.; Rheingold, A. L.; Figueroa, J. S. *Angew. Chem., Int. Ed.* **2009**, *48*, 3473–3477. (h) Sircoglou, M.; Mercy, M.; Saffon, N.; Coppel, Y.; Bouhadir, G.; Maron, L.; Bourissou, D. *Angew. Chem., Int. Ed.* **2009**, *48*, 3454–3457. (i) Gualco, P.; Lin, T.-P.; Sircoglou, M.; Mercy, M.; Ladeira, S.; Bouhadir, G.; Pérez, L. M.; Amgoune, A.; Maron, L.; Gabbai, F. P.; Bourissou, D. *Angew. Chem., Int. Ed.* **2009**, *48*, 9892–9895. (j) Wagler, J.; Brendler, E. *Angew. Chem., Int. Ed.* **2010**, *49*, 624–627. (k) Braunschweig, H.; Radacki, K.; Schwab, K. *Chem. Commun.* **2010**, 913–915. (l) Kolpin, K. B.; Emslie, D. J. H. *Angew. Chem., Int. Ed.* **2010**, *49*, 2716–2719. (m) Cowie, B. E.; Emslie, D. J. H.; Jenkins, H. A.; Britten, J. F. *Inorg. Chem.* **2010**, *49*, 4060–4072. (n) Wagler, J.; Brendler, E.; Langer, T.; Poettgen, R.; Heine, T.; Zhechkov, L. *Chem.—Eur. J.* **2010**, *16*, 13429–13434. (o) Truffandier, L. A.; Brendler, E.; Wagler, J.; Autschbach, J. *Angew. Chem., Int. Ed.* **2011**, *50*, 255–259. (p) Derrah, E. J.; Sircoglou, M.; Mercy, M.; Ladeira, S.; Bouhadir, G.; Miqueu, K.; Maron, L.; Bourissou, D. *Organometallics* **2011**, *30*, 657–660.
- (24) Becke, A. D.; Edgecombe, K. E. *J. Chem. Phys.* **1990**, *92*, 5397–5403.
- (25) (a) Meyer, N.; Lehmann, C. W.; Lee, T. K. M.; Rust, J.; Yam, V. W. W.; Mohr, F. *Organometallics* **2009**, *28*, 2931–2934. (b) Partyka, D. V.; Esswein, A. J.; Zeller, M.; Hunter, A. D.; Gray, T. G. *Organometallics* **2007**, *26*, 3279–3282. (c) Gao, L.; Peay, M. A.; Partyka, D. V.; Updegraff, J. B., III; Teets, T. S.; Esswein, A. J.; Zeller, M.; Hunter, A. D.; Gray, T. G. *Organometallics* **2009**, *28*, 5669–5681.
- (26) Schmidbaur, H.; Mitschke, K. H.; Buchner, W.; Stuehler, H.; Weidlein, J. *Chem. Ber.* **1973**, *106*, 1226–1237.
- (27) Sharutin, V. V.; Sharutina, O. K.; Pakusina, A. P.; Smirnova, S. A.; Pushilin, M. A. *Russ. J. Coord. Chem.* **2005**, *31*, 108–114.
- (28) Bordner, J.; Andrews, B. C.; Long, G. G. *Cryst. Struct. Commun.* **1976**, *5*, 801–804.
- (29) Neugebauer, W.; Clark, T.; Schleyer, P. v. R. *Chem. Ber.* **1983**, *116*, 3283–3292.
- (30) Kimura, M.; Iwata, A.; Itoh, M.; Yamada, K.; Kimura, T.; Sugiura, N.; Ishida, M.; Kato, S. *Helv. Chim. Acta* **2006**, *89*, 747–783.
- (31) Uson, R.; Laguna, A.; Laguna, M. *Inorg. Synth.* **1989**, *26*, 85–91.
- (32) (a) ADF2008.01, ADF2008.01. SCM, Theoretical Chemistry, Vrije Universiteit, Amsterdam, The Netherlands, <http://www.scm.com>. (b) Fonseca Guerra, C.; Snijders, J. G.; te Velde, G.; Baerends, E. J. *Theor. Chem. Acc. Theor. Comput. Model Theor. Chim. Acta* **1998**, *99*, 391–403. (c) te Velde, G.; Bickelhaupt, F. M.; Baerends, E. J.; Guerra, C. F.; Gisbergen, S. J. A. v.; Snijders, J. G.; Ziegler, T. *J. Comput. Chem.* **2001**, *22*, 931–967.
- (33) (a) Becke, A. D. *Phys. Rev. A* **1988**, *38*, 3098–3100. (b) Perdew, J. P. *Phys. Rev. B* **1986**, *33*, 8822–8824.
- (34) van Lenthe, E.; Baerends, E. J. *J. Comput. Chem.* **2003**, *24*, 1142–1156.
- (35) (a) van Lenthe, E.; Baerends, E. J.; Snijders, J. G. *J. Chem. Phys.* **1993**, *99*, 4597–4610. (b) van Lenthe, E.; Baerends, E. J.; Snijders, J. G. *J. Chem. Phys.* **1994**, *101*, 9783–9792. (c) van Lenthe, E.; Leeuwen, R. v.; Baerends, E. J.; Snijders, J. G. *Int. J. Quantum Chem.* **1996**, *57*, 281–293. (d) van Lenthe, E.; Snijders, J. G.; Baerends, E. J. *J. Chem. Phys.* **1996**, *105*, 6505–6516. (e) van Lenthe, E.; Ehlers, A.; Baerends, E.-J. *J. Chem. Phys.* **1999**, *110*, 8943–8953.
- (36) (a) Foster, J. M.; Boys, S. F. *Rev. Mod. Phys.* **1960**, *32*, 300–302. (b) Edmiston, C.; Ruedenberg, K. *Rev. Mod. Phys.* **1963**, *35*, 457–464. (c) Von Niessen, W. *J. Chem. Phys.* **1972**, *56*, 4290–4297.
- (37) Bruker, SAINTPlus. *Data Reduction and Correction Program*, v. 6.2; Bruker AXS: Madison, Wisconsin, USA, 2001.
- (38) Sheldrick, G. M. SHELXTL-2008/2004, *Structure Determination Software Suite*; Bruker AXS, Madison, Wisconsin, USA, 2008.
- (39) Spek, A. L. PLATON, A Multipurpose Crystallographic Tool; Utrecht University: Utrecht, The Netherlands, 1998.